

8-1-2011

# CONSTITUTIVE MODEL FOR RATE DEPENDENT BEHAVIOR OF CLAY Internal Geotechnical Report 2011-3


Harry Martindale

*University of Connecticut - Storrs, [harry.martindale@uconn.edu](mailto:harry.martindale@uconn.edu)*

Dipanjan Basu

*University of Connecticut - Storrs, [dipanjan.basu@uconn.edu](mailto:dipanjan.basu@uconn.edu)*

Follow this and additional works at: [https://opencommons.uconn.edu/cee\\_techreports](https://opencommons.uconn.edu/cee_techreports)

 Part of the [Civil Engineering Commons](#), [Environmental Engineering Commons](#), and the [Geotechnical Engineering Commons](#)

## Recommended Citation

Martindale, Harry and Basu, Dipanjan, "CONSTITUTIVE MODEL FOR RATE DEPENDENT BEHAVIOR OF CLAY Internal Geotechnical Report 2011-3" (2011). *Technical Reports*. 3.  
[https://opencommons.uconn.edu/cee\\_techreports/3](https://opencommons.uconn.edu/cee_techreports/3)

**CONSTITUTIVE MODEL FOR RATE DEPENDENT BEHAVIOR OF  
CLAY**

*Internal Geotechnical Report 2011-3*

Harry Martindale and Dipanjan Basu

Department of Civil and Environmental Engineering  
University of Connecticut

Storrs, Connecticut

August 2011

Copyright by

Harry Martindale and Dipanjan Basu

2011

## SYNOPSIS

This report presents a strain-rate dependent plastic constitutive model for clays. Based on the concepts of critical-state soil mechanics and bounding surface plasticity theory, the model reproduces the mechanical response of clays under multi-axial loading conditions and predicts both the drained and undrained behavior. The model parameters are determined for Boston Blue Clay, London Clay and Kaolin Clay, and the performance of the model in simulating the mechanical response of these clays is demonstrated for low to medium strain rates. The sensitivity of each model parameter is checked by perturbing the calibrated values by  $\pm 20\%$ . Subsequently, a probabilistic analysis using Monte Carlo simulations is performed by treating the model parameters as random variables and the impact of the statistics of the parameters on the undrained shear strength is investigated.

**KEYWORDS:** Constitutive relations; Plasticity; Rate-dependence; Clay; Probabilistic analysis

## INTRODUCTION

The mechanical behavior of clayey soils is affected by the rate of induced strains (Kavazanjian and Mitchell 1980, Sorensen et al. 2007, Sheahan 2005 and 1991, Díaz-Rodríguez et al. 2009, Matesic and Vucetic 2003). Examples of practical problems where rate-dependent behavior of clay is important are landslides, pile penetration and wave loads on offshore foundations. The rate effects in clay are exhibited from a low applied strain rate of  $10^{-2}\%/hr$  ( $\approx 10^{-7}/sec$ ). It has been observed in the laboratory triaxial compression tests that, for low to medium applied strain rates of  $10^{-2}$ - $10^2\%/hr$  ( $\approx 10^{-7}$ - $10^{-4}/sec$ ), the undrained shear strength increases by 5-20% per log-cycle increase in the strain rate. The initial shear modulus increases at a rate of about 10% per log-cycle increase in the applied strain rate (Matesic and Vucetic 2003). The critical-state strength of clays, however, remains rather unaffected by the rate of induced strains under low to medium strain rates (Sheahan et al. 1996, Sorensen et al. 2007, Díaz-Rodríguez et al. 2009). The overconsolidation ratio (*OCR*) plays an important role in the rate-dependent mechanical response of clay. For a constant *OCR*, the deviatoric stress attains its peak at approximately the same strain level for different strain rates. However, the strain at which the peak occurs increases with increasing *OCR*. Significant post-peak softening is observed for low *OCR* of 1 and 2 due to the generation of positive excess pore pressure while, for *OCR* of 4 or greater, the post-peak softening is relatively small.

Rate dependence of clay has been mostly investigated for creep and stress relaxation, and elasto-viscoplastic constitutive models based on overstress theory have been developed to simulate them (Perzyna 1963, 1966, Zienkiewicz and Cormeau 1974, Adachi and Oka 1982, Hinchberger and Rowe 1998). Adachi and Oka (1982) proposed

an elasto-viscoplastic constitutive model based on the original Cam-clay model to capture creep, stress relaxation and secondary consolidation. Hinchberger and Rowe (1998) incorporated Perzyna's overstress theory in elliptical Drucker-Prager cap model to capture the secondary consolidation behavior of clay. Viscoplasticity has been combined with the bounding surface plasticity theory as well to simulate creep, stress relaxation and secondary compression of normally-consolidated (NC) and overconsolidated (OC) clays (Dafalias 1982, Kaliakin and Dafalias 1990a, b).

The constitutive models developed to model clay subjected to induced strain rates are mostly different from the above viscoplastic models. Clays subjected to rate-dependent strains have been mostly modeled using explicit strain-rate dependent equations without the use of viscoplastic overstress theories. In these models, the relevant clay properties (e.g., peak undrained shear strength) are explicitly expressed as functions of the applied strain rates where the applied strain rate is a model input parameter, and the rate-independent plasticity theory is used to simulate the rate-dependent behavior (Jung and Biscontin 2006, Zhou and Randolph 2007 and Chakraborty 2009). These constitutive models do not involve numerically expensive viscoplastic stress-strain integration scheme and can predict the strain-rate dependent behavior with reasonable accuracy.

In this report, a constitutive model is presented that simulates the mechanical response of clay subjected to strains applied with a rate of up to 50%/hr ( $\approx 1 \times 10^{-4}$ /sec). Based on the concepts of critical state soil mechanics and bounding surface plasticity theory, the model incorporates the rate effects under various loading conditions in the multiaxial stress space. The model is an extension of the bounding surface plasticity

model developed by Manzari and Dafalias (1997) and later modified by Li and Dafalias (2000), Papadimitriou and Bouckovalas (2002), Dafalias et al. (2004), Loukidis and Salgado (2009) and Chakraborty (2009). The model parameters have been determined for Boston Blue Clay (BBC), London Clay (LC) and Kaolin Clay (KC) by comparing the simulation results with the experimental data available in the literature. The rate-dependent model parameter is determined from the strain-rate dependent triaxial compression test data, while the rate-independent parameters are determined from one-dimensional and isotropic consolidation tests, resonant column tests, triaxial compression and extension tests, and simple shear tests following a hierarchical process. A sensitivity analysis is performed by varying the input model parameters by  $\pm 20\%$  of the calibrated values. Finally, a probabilistic analysis is performed by treating the input model parameters as random variables and performing Monte Carlo simulations, and the statistics of the output undrained shear strength is investigated.

## **CONSTITUTIVE MODEL DEVELOPMENT**

### ***Model Surfaces in Stress Space***

The basic, rate-independent part of the model consists of yield, dilatancy, and critical-state surfaces that are made up of two distinct geometrical surfaces: a cone with straight surfaces in the meridional plane and apex at the origin, and a bounding flat cap on the critical state surface (Chakraborty 2009). The model formulation is done in terms of stress ratios, i.e., stresses normalized with respect to the mean effective stress  $p'$  ( $= \sigma'_{kk}/3$ , where  $\sigma'_{ij}$  is the effective Cauchy stress tensor). Figure 1(a) shows the projection of the yield, dilatancy and critical-state surfaces on the  $\pi$ -plane of the principal deviatoric stress ratio space  $s_1/p'-s_2/p'-s_3/p'$  ( $s_{ij} = \sigma'_{ij} - \delta_{ij}\sigma'_{kk}/3$  is the deviatoric stress tensor in

which  $\delta_{ij}$  denotes the Kronecker's delta). Figure 1(b) shows the projection of the model surfaces on the longitudinal  $q$ - $p'$  plane ( $q = \sigma'_1 - \sigma'_3$  is the deviatoric stress in the triaxial stress space). The yield surface is expressed in terms of the deviatoric stress ratio tensor  $r_{ij}$  ( $= s_{ij}/p'$ ) as

$$f = \sqrt{(r_{ij} - \alpha_{ij})(r_{ij} - \alpha_{ij})} - \sqrt{2/3} m = 0 \quad (1)$$

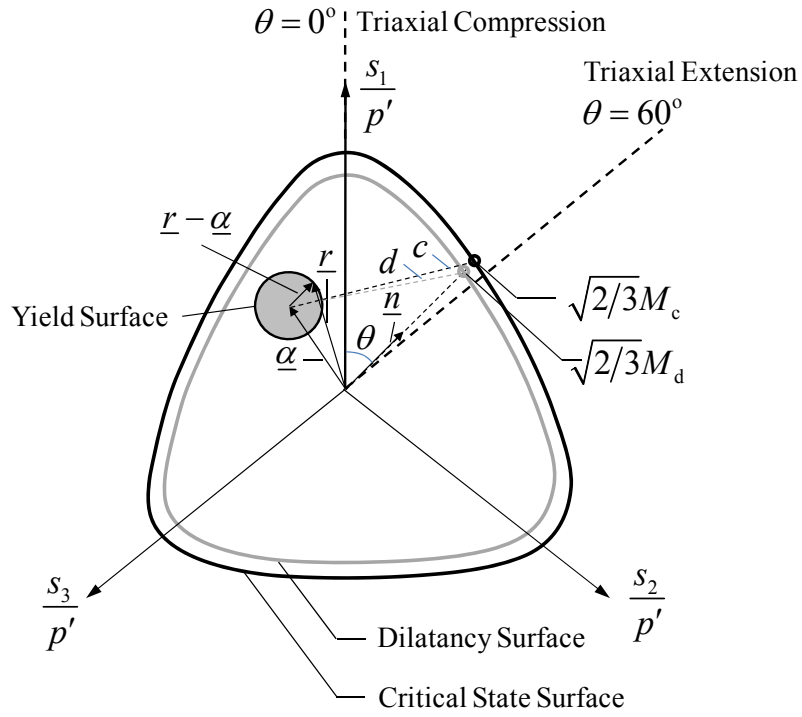
which can be visualized as a cone in the principal deviatoric stress space intersecting the  $\pi$ -plane as a circle with radius  $\sqrt{2/3}m$  and center  $\alpha_{ij}$ , which is the kinematic hardening tensor. The yield surface cannot harden isotropically (i.e.,  $m$  stays constant in the model) but can harden kinematically through the evolution of  $\alpha_{ij}$  given by

$$\dot{\alpha}_{ij} = \dot{\lambda}_{\text{shear}} \frac{H_s}{p'} \left( \sqrt{\frac{2}{3}} (M_c - m) n_{ij} - \alpha_{ij} \right) / \left( \sqrt{\frac{2}{3}} (M_c - m) - \alpha_{ij} n_{ij} \right) \quad (2)$$

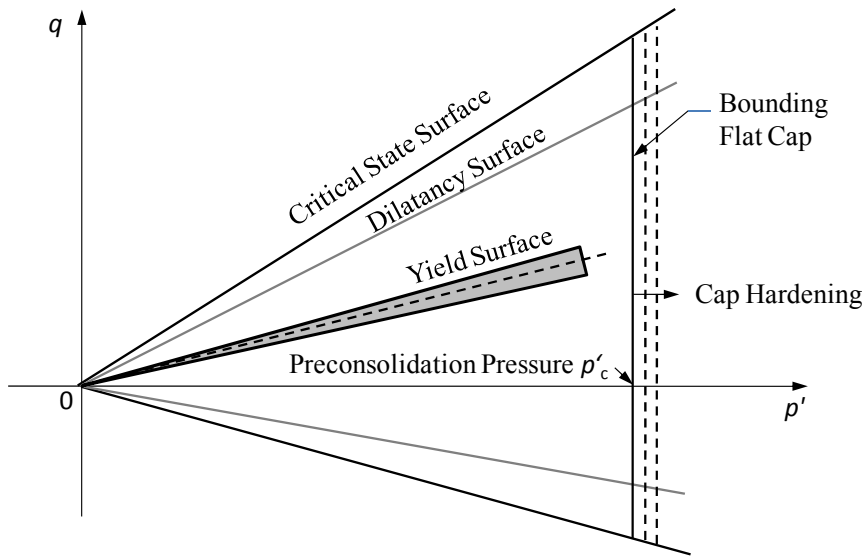
where  $\dot{\lambda}_{\text{shear}}$  is the shearing-related plastic multiplier,  $H_s$  is the plastic modulus controlling the development of the plastic shear strain (the equations of  $\dot{\lambda}_{\text{shear}}$  and  $H_s$  are given later),  $n_{ij} \left[ = (s_{ij} - p'\alpha_{ij}) / \sqrt{(s_{kl} - p'\alpha_{kl})(s_{kl} - p'\alpha_{kl})} \right]$  determines the direction of the projection of the current stress on the critical-state and dilatancy surfaces (i.e., the mapping rule) and  $M_c$  denotes the critical-state surface defined by

$$M_c = g(\theta) M_{cc} = \left[ \frac{\left( 1 - \frac{1 - c_1^{1/n_s}}{1 + c_1^{1/n_s}} \right)^{n_s}}{\left( 1 - \frac{1 - c_1^{1/n_s}}{1 + c_1^{1/n_s}} \cos 3\theta \right)^{n_s}} \right] M_{cc} \quad (3)$$





(a)



(b)

Figure 1. Plastic constitutive model plotted in (a) the deviatoric plane and (b) the meridional plane

where  $M_{cc}$  is the stress ratio  $q/p'$  at the critical-state (CS) under triaxial compression,  $g(\theta)$  is a function of the Lode's angle  $\theta$  and determines the shape of the critical state surface in the deviatoric stress space and  $c_1 = 3/(M_{cc} + 3)$ . The parameter  $n_s$  takes a constant value of 0.2 for all the clays. The dilatancy surface is defined by

$$M_d = g(\theta) \left[ 2M_{cc} + \frac{M_{cc} k_d \xi OCR}{1 - \exp(k_d \xi OCR)} \right] \quad (4)$$

where  $\xi = e - e_{CS}$  is the state parameter (Been and Jefferies 1985) in which  $e$  and  $e_{CS}$  are the current and critical-state void ratios at the same mean stress (Figure 2),  $OCR$  is the overconsolidation ratio and  $k_d$  is given by

$$k_d = \frac{M_{cc}}{(\lambda - \kappa) \ln \rho} \quad (5)$$

in which  $\lambda$  and  $\kappa$  are the slopes of the linear normal-consolidation and overconsolidation lines in the  $e$ - $\ln(p')$  space and  $\rho (= p'_c/p'_{CS})$  is the ratio of the preconsolidation pressure  $p'_c$  to the critical-state pressure  $p'_{CS}$  along the same overconsolidation line in the  $e$ - $\ln(p')$  space (Figure 2). The dilatancy surface hardens isotropically as the state parameter  $\xi$  changes due to a change in the stress state.

The flat cap to the critical-state surface helps in capturing the yielding and development of plastic strains under pure compression. The bounding flat cap is perpendicular to the hydrostatic (mean stress) axis and intersects the hydrostatic axis at  $p' = p'_c$  (Figure 1b). It is given by

$$F_c = p' - p'_c = 0 \quad (6)$$

The movement of the cap along the mean-stress axis signifies the increase in the preconsolidation pressure along the normal consolidation line (*NCL*) in the  $e$ - $\ln(p')$  space.

The consistency condition is not applied to the cap, and hence, stress states marginally outside the cap are possible.

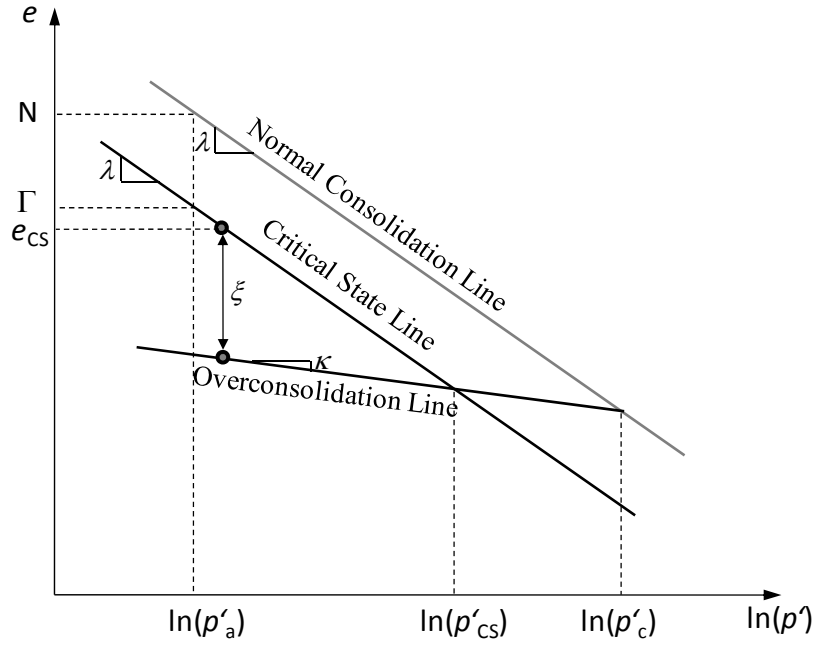


Figure 2. Locus of the normal consolidation line and critical state line in  $e$ - $\ln(p')$  space

The normal consolidation line is given by (Figure 2)

$$e_{\text{NC}} = N - \lambda \ln \left( \frac{p'}{p'_a} \right) \quad (7)$$

where  $e_{\text{NC}}$  is the normal consolidation void ratio and  $N$  is the void ratio at the reference mean stress  $p_a$  ( $= 100$  kPa). The critical state line (CSL) follows the same slope as that of the normal consolidation line in the  $e$ - $\ln(p')$  space, and is given by

$$e_{\text{CS}} = \Gamma_0 - \lambda \ln \left( \frac{p'}{p_a} \right) = N - (\lambda - \kappa) \ln \rho - \lambda \ln \left( \frac{p'}{p_a} \right) \quad (8)$$

where  $\Gamma_0$  is the critical state void ratio at the reference mean stress  $p_a$  under rate-independent loading.

The *NCL* of clays under rate-independent loading lies to the left of the rate-dependent *NCL* in the  $e-\ln(p')$  space, and the rightward shift of the *NCL* happens with increase in the rate of the applied strain (Leroueil et al. 1985, Sheahan 2005). This movement of *NCL* as a function of strain rate signifies an increase in the preconsolidation pressure  $p'_c$  with increase in the strain rate. Based on the available experimental results, the rate dependent preconsolidation pressure  $p'_{c,rd}$  is found to be a function of the applied strain rate  $\dot{\epsilon}_{ij}$  and can be expressed in terms of an equivalent strain rate  $\dot{\epsilon}_{eq} (= \sqrt{\dot{\epsilon}_{ij}\dot{\epsilon}_{ij}})$  as (Figure 3)

$$p'_{c,rd} = p'_{c,ri} \left( 1.3 \dot{\epsilon}_{eq}^{0.05} \right) \quad (9)$$

where  $p'_{c,ri}$  is the rate-independent value of the preconsolidation pressure and  $\dot{\epsilon}_{eq}$  is expressed in %/hr.

Experimental studies also show that the peak undrained strength increases with increasing strain rate. This increase is captured by the model in a simple but practical way by assuming that the critical state line moves to the right in the  $e-\ln(p')$  space with increasing strain rate (Chakraborty 2009). Mathematically, this is achieved by replacing  $\Gamma_0$  in the equation of critical state line [equation (8)] with  $\Gamma$  given by

$$\Gamma = \Gamma_0 \left[ 1 + C_0 \ln(0.1 C_0 \dot{\epsilon}_{eq} + 1) \ln(d_c + 1) \right] \quad (10)$$

where  $C_0$  is a model parameter,  $d_c$  denotes a distance in the three-dimensional void ratio-mean stress-deviatoric space between the current soil state and the critical state and  $\dot{\epsilon}_{eq}$  is expressed in %/hr. Thus,  $\Gamma = \Gamma_0$  when  $\dot{\epsilon}_{eq} = 0$ . The distance  $d_c$  is defined as

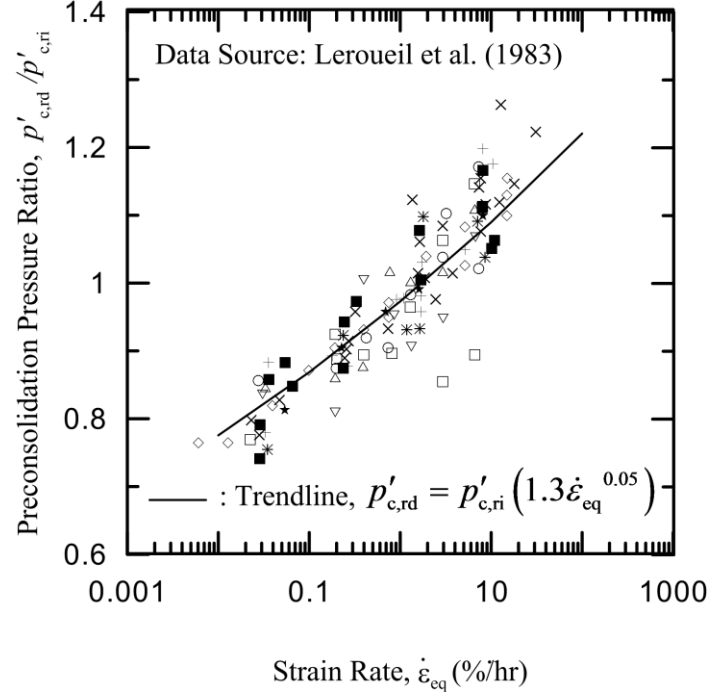


Figure 3. Preconsolidation pressure as a function of strain rate

$$d_c = \sqrt{C_0 \left[ \xi_{ini}^2 + (\bar{d})^2 \right]} \quad (11)$$

where  $\xi_{ini}$  is the initial value of the state parameter and  $\bar{d}$  is a normalized distance of the current stress state from the critical-state surface in the deviatoric plane.  $\bar{d}$  is given by

$$\bar{d} = \frac{\left\langle M_c - \sqrt{\frac{3}{2}} \sqrt{r_{ij}^* r_{ij}} \right\rangle}{M_c} \quad (12)$$

In this model, the *NCL* and *CSL* move independently as the strain rate increases, but the *CSL* does not cross the *NCL*.

### ***Elastic Shear and Bulk Moduli***

The stress-strain relation is given by

$$\dot{\sigma}'_{ij} = 2G(\dot{\epsilon}'_{ij} - \dot{\epsilon}^p_{ij}) + \left(K - \frac{2}{3}G\right)(\dot{\epsilon}'_{kk} - \dot{\epsilon}^p_{kk})\delta_{ij} \quad (13)$$

where the total strain rate  $\dot{\epsilon}'_{ij}$  has an elastic ( $\dot{\epsilon}^e_{ij}$ ) and a plastic ( $\dot{\epsilon}^p_{ij}$ ) component [ $\dot{\epsilon}'_{ij} = \dot{\epsilon}^e_{ij} + \dot{\epsilon}^p_{ij}$ ], and  $G$  and  $K$  are the shear and bulk moduli, respectively. When the stress state is entirely within the yield surface, there is no plastic strain in the soil. Since the yield surface is very small in this model, the plastic process is prevalent for almost the entire loading duration.

$G$  and  $K$  are assumed to decrease exponentially with increasing shear and/or mean stresses from the initial values  $G_{\max}$  and  $K_{\max}$  until certain minimal values  $G_{\min}$  and  $K_{\min}$  are reached:

$$G = G_{\min} + (G_{\max} - G_{\min}) \exp \left[ -\zeta \left( \frac{|p' - p'_{ini}|}{p'_c} + \frac{\sqrt{3/2} \sqrt{(r_{ij} - \alpha_{ij,ini})(r_{ij} - \alpha_{ij,ini})}}{M_{cc}} \right) \right] \quad (14)$$

$$K = K_{\min} + (K_{\max} - K_{\min}) \exp \left[ -\zeta \left( \frac{|p' - p'_{ini}|}{p'_c} + \frac{\sqrt{3/2} \sqrt{(r_{ij} - \alpha_{ij,ini})(r_{ij} - \alpha_{ij,ini})}}{M_{cc}} \right) \right] \quad (15)$$

where  $p'_{ini}$  is the initial mean stress,  $\zeta$  is a model parameter and  $\alpha_{ij,ini}$  is the initial value of kinematic hardening tensor. The small-strain shear modulus  $G_{\max}$  is given by (Hardin 1978)

$$G_{\max} = C_g \frac{(2.97 - e)^2}{1 + e} \sqrt{p' p'_a} (OCR)^{0.2} \quad (16)$$

where  $C_g$  is a material parameter. The initial bulk modulus  $K_{\max}$  is related to the small-strain shear modulus  $G_{\max}$  through a constant Poisson's ratio  $\nu$  as

$$K_{\max} = G_{\max} \frac{2(1+\nu)}{3(1-2\nu)} \quad (17)$$

The minimal values of bulk and shear moduli,  $K_{\min}$  and  $G_{\min}$ , are given by

$$K_{\min} = \frac{p'(1+e)}{\kappa} \quad (18)$$

$$G_{\min} = \frac{3(1-2\nu)}{2(1+\nu)} K_{\min} \quad (19)$$

which are obtained using the slope  $\kappa$  of the overconsolidation lines in the  $e-\ln(p')$  space observed in one-dimensional compression tests for a constant Poisson's ratio  $\nu$ .

### **Flow Rule**

The plastic strain tensor  $\varepsilon_{ij}^p$  has two components:  $\varepsilon_{ij,\text{shear}}^p$  and  $\varepsilon_{ij,\text{cap}}^p$ . The component  $\varepsilon_{ij,\text{shear}}^p$  is related to the conical yield, dilatancy and critical state surfaces, and its rate is given by

$$\dot{\varepsilon}_{ij,\text{shear}}^p = \dot{\lambda}_{\text{shear}} R_{ij} = \dot{\lambda}_{\text{shear}} \left( R'_{ij} + \frac{1}{3} D \delta_{ij} \right) \quad (20)$$

The gradient  $R_{ij}$  of the plastic potential in the stress space is assumed to consist of a deviatoric component  $R'_{ij}$  (given in Loukidis and Salgado 2009 and Chakraborty 2009), which expresses the direction of the deviatoric plastic strain rate  $\dot{\varepsilon}_{ij,\text{shear}}^p$ , and a mean component related directly to the dilatancy  $D$  that controls the shear-induced plastic volumetric strain rate  $\dot{\varepsilon}_{kk,\text{shear}}^p$ . The dilatancy  $D$  is given by

$$D = \frac{d_0}{M_{\text{cc}} OCR} \left[ \sqrt{\frac{2}{3}} (M_d - m) - \alpha_{ij} n_{ij} \right] \left[ 1 + \ln(\dot{\varepsilon}_{\text{eq}} + 1) \right] \exp[d_1 (1 - OCR)] \quad (21)$$

and it depends on the “distance”  $d (= \sqrt{2/3}(M_d - m) - \alpha_{ij}n_{ij})$  between the current and projected stress states on the dilatancy surface (Figure 1a) and on the strain rate. The unit vector  $n_{ij}$  is parallel to the vector connecting the center of the yield surface in the  $\pi$ -plane (i.e., the axis of the yield surface) to the current stress point on the yield surface (Figure 1a).  $n_{ij}$  determines the image stresses on the critical-state and dilatancy surfaces, and hence, determines the direction of projection of the current stress on the critical-state and dilatancy surfaces. The parameter  $d_0$  controls the development of  $D$  with stress ratio. The parameter  $d_1$  controls the dependence of dilatancy on  $OCR$ . The plastic multiplier  $\dot{\lambda}_{\text{shear}}$  for yielding in the shearing mode is obtained by satisfying the consistency condition for the conical yield surface and is given by

$$\dot{\lambda}_{\text{shear}} = \frac{1}{H_s} \frac{\partial f}{\partial \sigma'_{ij}} \dot{\sigma}'_{ij} = \frac{1}{H_s} \left( n_{ij} - \frac{1}{3} (n_{kl} r'_{kl}) \delta_{ij} \right) \dot{\sigma}'_{ij} \quad (22)$$

The plastic modulus  $H_s$  in the above equation, controlling the development of  $\varepsilon_{ij,\text{shear}}^p$ , is given by

$$H_s = h_0 \frac{G \times OCR}{\left[ \sqrt{\frac{3}{2}} \sqrt{(r_{ij} - \alpha_{ij,\text{ini}})(r_{ij} - \alpha_{ij,\text{ini}})} \right]} \sqrt{\frac{2}{3}} \left( \sqrt{\frac{2}{3}} (M_c - m) - \alpha_{ij} n_{ij} \right) \quad (23)$$

$H_s$  depends on the distance between the current stress state and the image stress state on the critical-state surface (represented by  $c$  in Figure 1a).

The second component of plastic strain,  $\varepsilon_{ij,\text{cap}}^p$ , is given by

$$\dot{\varepsilon}_{ij,\text{cap}}^p = \frac{\dot{\lambda}_{\text{cap}}}{D^*} \left( R'_{ij} + \frac{1}{3} \delta_{ij} D^* \right) \quad (24)$$



where  $D^*$  is the cap related dilatancy and  $\dot{\lambda}_{\text{cap}}$  the cap related plastic multiplier (Chakraborty 2009). The equation of  $D^*$  is obtained by Chakraborty (2009) as

$$D^* = \left[ \frac{1}{p'} \frac{\lambda - \kappa}{1 + e} \right] \left( \frac{1 - K_{0,\text{NC}}}{\frac{1}{3}(1 + 2K_{0,\text{NC}})} \sqrt{r_{ij}^* r_{ij}} \right) / \left[ \frac{1}{K} + \frac{1}{p'} \frac{\lambda - \kappa}{1 + e} - \frac{1 - K_{0,\text{NC}}}{\frac{1}{3}(1 + 2K_{0,\text{NC}})} \frac{1}{2G} \right] \quad (25)$$

where  $K_{0,\text{NC}}$  is the coefficient of earth pressure at rest for normally consolidated clay.

$\dot{\lambda}_{\text{cap}}$  is given by

$$\dot{\lambda}_{\text{cap}} = \frac{1}{H_c} \langle \dot{p}' \rangle \quad (26)$$

where  $H_c$  is the plastic modulus controlling the development of  $\varepsilon_{ij,\text{cap}}^p$  and is given by

$$H_c = p' \frac{1 + e}{\lambda - \kappa} \exp \left[ \zeta \frac{p'_c - p'}{p'} \right] \quad (27)$$

$H_c$  is very high for stress states far from the cap but decreases exponentially with the distance  $p'_c - p'$ .

The constitutive model presented in this report is an extension of previously developed constitutive model by Manzari and Dafalias (1997), Dafalias et al. (2004), Loukidis and Salgado (2009) and Chakraborty (2009). The unique features of the constitutive model presented herein are (1) a new equation for the strain-rate dependent preconsolidation pressure, (2) use of a single parameter  $C_0$  to capture the rate dependence as a function of  $OCR$ , (3) variable distance between  $CSL$  and  $NCL$  in the  $e - \ln(p')$  space and (4) rate dependent dilatancy equation. These features have improved the performance of the model significantly.

The stress-strain integration of the constitutive model is performed using an elastic predictor-plastic corrector algorithm as illustrated in Figure 4 (Ortiz and Simo 1986). In this algorithm, at a certain time step  $t = t_i$ , the stresses  $\sigma'_{ij}$ , kinematic hardening variable  $\alpha_{ij}$  and void ratio  $e$  are the input parameters. The elastic predictor stress is calculated from the input stresses using the strain increment  $\Delta\epsilon_{kl}$  in the iteration step. The elastic stiffness matrix  $D_{ijkl}^{el}$  used in the stress-strain relation is the shear modulus when deviatoric stress is calculated from deviatoric strain and is the bulk modulus when mean stress is calculated from volumetric strain. Once the elastic predictor stresses are calculated, the yield stress value  $f$  is checked with the yield surface error tolerance  $FTOL$  ( $= 10^{-9}$ ). If  $f < FTOL$ , it signifies that the stresses are elastic and the iteration loop completes and the next strain increment starts. If  $f > FTOL$ , then stresses are outside the yield surface, and plastic correction starts. Plastic multiplier  $\dot{\lambda}$  is calculated to perform the plastic correction. The shear induced plastic multiplier  $\dot{\lambda}_{shear}$  is calculated for the deviatoric stress correction and the cap induced plastic multiplier  $\dot{\lambda}_{cap}$  is calculated for the cap induced volumetric stress correction. In the correction step, the total incremental strain  $\Delta\epsilon_{kl}$  for that particular increment remains constant. After the stress correction is done, stresses, kinematic hardening variable and void ratio are updated and the yield stress value is again checked with  $FTOL$ . Further plastic correction is performed before starting a new strain increment if  $f > FTOL$ . For the simulation of the rate-independent, single element triaxial test, one-step plastic correction iteration is generally sufficient when the incremental strain  $\Delta\epsilon_{kl}$  is sufficiently small. However, for simulating rate-

dependent behavior, 3-5 correction iterations are necessary depending on the applied strain rate.

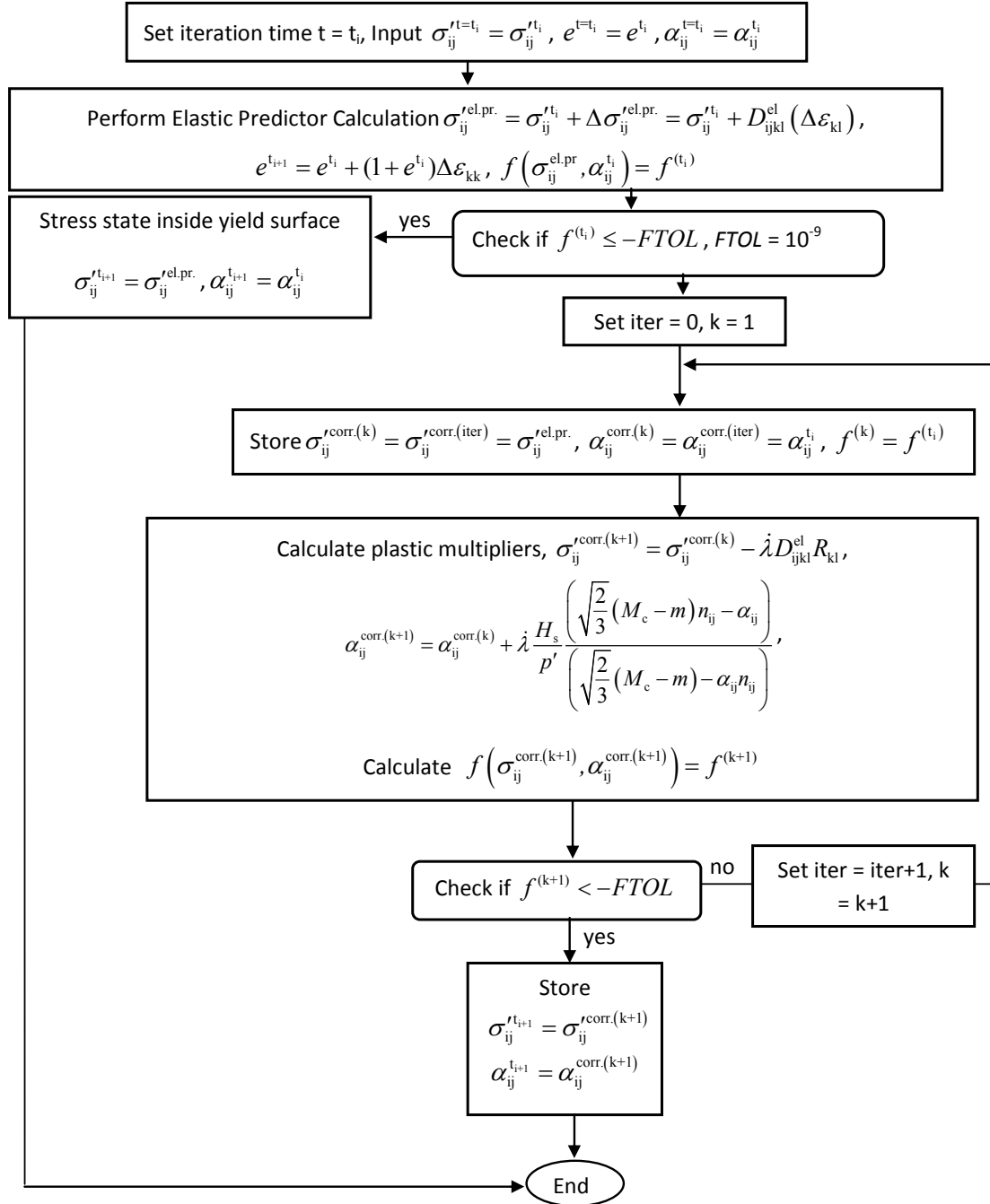


Figure 4. Flowchart for the elastic predictor-plastic corrector algorithm used for stress-strain integration of the constitutive model

## MODEL PARAMETERS

The constitutive model has 14 rate-independent and 1 rate-dependent parameters. These parameters were determined based on one-dimensional consolidation, triaxial compression and extension, simple shear, bender element and resonant column tests. The constitutive model is calibrated in a hierarchical manner by curve fitting over given sets of experimental data points. Such a hierarchical process of model parameter determination is described in details in Chakraborty (2009).

The model parameters are determined for Boston Blue Clay (BBC), Kaolin Clay (KC), and London Clay (LC). BBC is a low-plasticity marine clay, composed of illite and quartz (Terzaghi et al. 1996). LC contains illite, kaolinite, smectite and quartz (Gasparre et al. 2007a and 2007b). KC mainly contains kaolinite. Table 1 shows the index properties of BBC, LC and KC. The calibrated values of the model parameters are given in Table 2. Most of the rate-independent model parameters for BBC and LC are obtained from Chakraborty (2009). The newly introduced dilatancy parameter  $d_1$  is determined by comparing the rate-independent simulation results with the experimental data obtained from the literature. The parameter  $\rho$  is recalibrated to better capture the anisotropic stress-strain behavior of clays. The experimental data for BBC used in this study are obtained from Papadimitriou et al. (2005), Pestana et al. (2002) and Ling et al. (2002) (the original test data of Ladd and Varallay 1965, Ladd and Edgers 1972 and Sheahan 1991 were used). The data for LC are obtained from Gasparre (2005), Gasparre et al. (2007a, b) and Hight et al. (2003). The experimental data for KC are obtained from Ling et al. (2002).

Table 1. Index Properties of Boston Blue Clay, London Clay, and Kaolin Clay

Clay Type	Liquid Limit (%)	Plastic Limit (%)	Classification	Reference
Boston Blue Clay	32.6	19.5	Inorganic Clay or Silt of Low to Medium Plasticity (CL) (USCS)	Ladd and Varallyay (1965)
London Clay	69.6	26.2	High Plasticity Stiff Clay	Nishimura (2005)
Kaolin Clay	62	30	Low Compressibility (CL/ML) (USCS)	Prashant (2004)

Table 2. Constitutive Model Parameters for Boston Blue Clay, London Clay and Kaolin Clay

Model Parameters				
Model Relationships		BBC	LC	KC
Small-Strain (Elastic) Poisson's ratio	$\nu$	0.25	0.2	0.25
$G_0$ Correlation Parameter	$C_g$	250	100	120
Elastic Moduli with Degradation	$\zeta$	5	10	5
	$\kappa$	0.036	0.064	0.033
Normal Consolidation Line	$N$	1.138	1.07	0.984
	$\lambda$	0.187	0.168	0.18
Critical State Surface	$M_c$	1.305	0.827	1.18
	$\rho$	2.2	2.5	2.7
Dilatancy Surface	$d_1$	0.2	0.2	0.2
	$d_0$	1	0.24	0.8
Flow Rule	$c_2$	0.95	0.95	0.95
	$n_s$	0.2	0.2	0.2
Hardening	$h_0$	1.1	1.1	1.1
Rate Dependence	$C_0$	0.1-2.0	2.0	0.05

The rate-dependent parameter  $C_0$  was determined by comparing the simulation results with the rate-dependent triaxial compression data of Sheahan (1991) and Sheahan et al. (1996) for BBC, of Sorensen et al. (2007) for LC and of Mukabi and Tatsuoka

(1999) for KC. It was observed for BBC that assuming one value of  $C_0$  for different  $OCR$ s did not produce good match with the experimental results. A similar observation was made by Hajek et al. (2009) who found that the constitutive equations that captured the behavior of normally consolidated clays did not capture the behavior overconsolidated clays well. Therefore, Hajek et al. (2009) considered an  $OCR$ -dependent model calibration process. Following a similar approach,  $C_0$  is assumed to be  $OCR$  dependent in this study. It was observed that only BBC required an  $OCR$  dependent calibration for  $C_0$  the values of which are given in Table 3. For LC and KC,  $C_0$  was found not to vary with  $OCR$  (Table 2).

Table 3. Rate Dependent Model Parameter  $C_0$  for Boston Blue Clay

$OCR$	Strain-rate (%/hr)	$C_0$
1	50	0.6
	5	1.1
	0.5	2.0
	0.05	2.0
2	50	0.55
	5	1.05
	0.5	2.0
	0.05	2.0
4	0.05-50	0.1
8	0.05-50	0.1

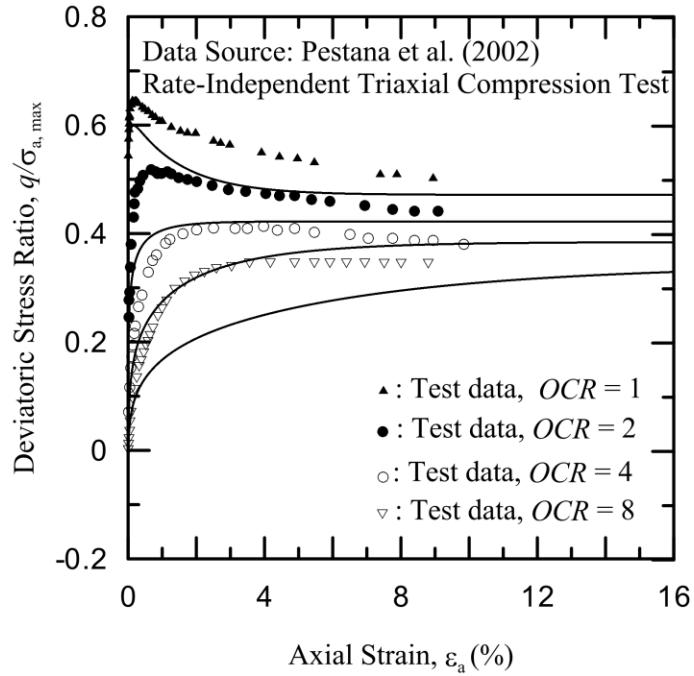
## MODEL SIMULATIONS

### *Undrained Rate-Independent Behavior*

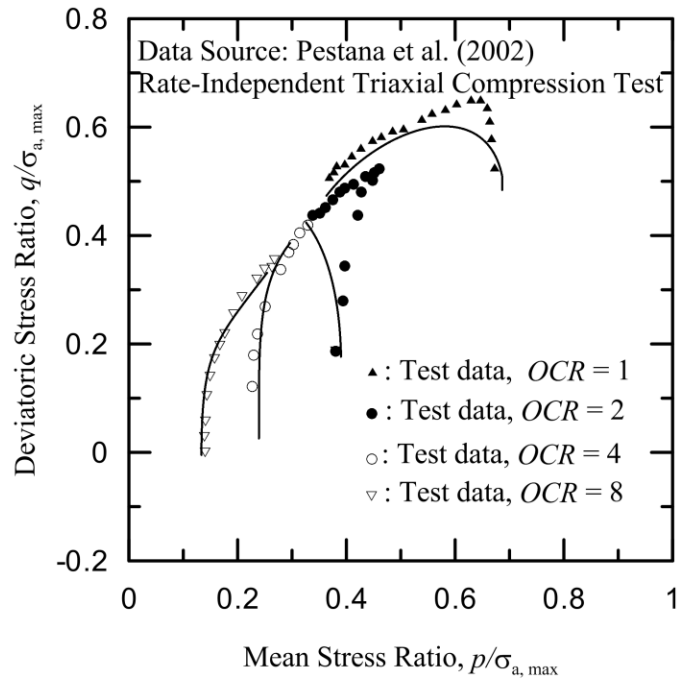
Figure 5 shows the rate-independent response of BBC as obtained from the model simulations and triaxial experiments. Figure 5(a) compare the model predictions with the

experimental data of the deviatoric stress  $q$  as a function of axial strain  $\varepsilon_a$  for undrained triaxial compression of  $K_0$ -consolidated specimens. Figure 5(b) shows the comparisons for the corresponding stress path plots (deviatoric stress versus mean stress). The stress values are normalized with respect to the maximum axial stress  $\sigma'_{a,max}$ . In the simulations, the same  $M_{cc}$  value is used for both isotropic and  $K_0$  consolidation cases. This causes a slight under prediction of stresses at  $OCR = 4$  and  $8$ . Overall, the simulations match the experimental results reasonably well. Similar match between experimental and simulation results were observed for LC and KC as well and are given in Martindale (2011).

Figure 6 compares the model predictions with the rate-independent experimental data of undrained triaxial compression tests performed on isotropically-consolidated specimens of LC. The stress-strain (Figures 6(a)) and stress path plots (Figure 6(b)) show a reasonable match between simulation results and experimental data. Similar comparisons for BBC and KC were also done and a reasonable match between experimental and simulation results were observed (Martindale 2011).



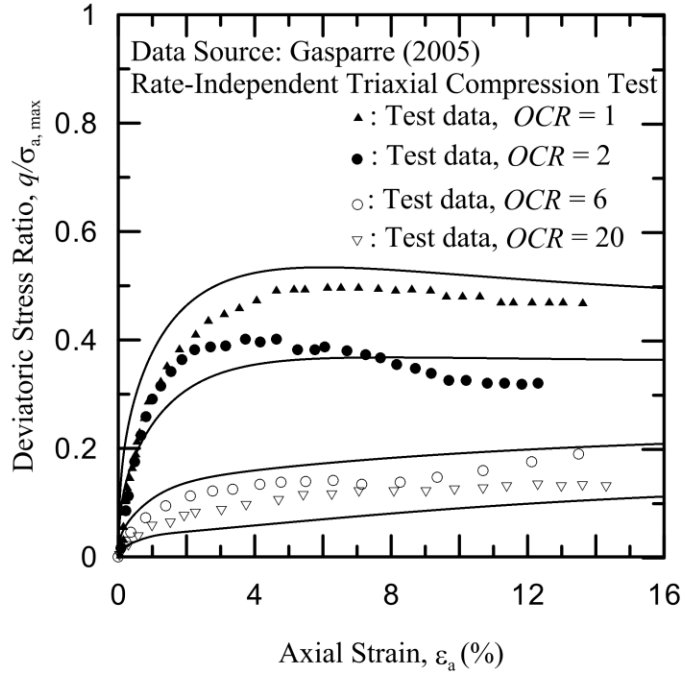
(a)



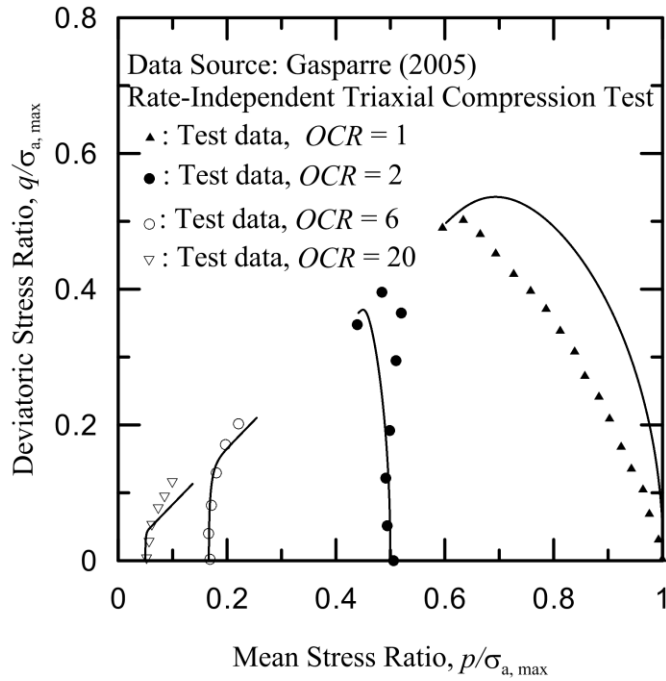
(b)

Figure 5. Rate-independent,  $K_0$  consolidated triaxial compression test results for Boston Blue Clay: (a) stress strain plot and (b) stress path plot (test data from Pestana et al. 2002)





(a)



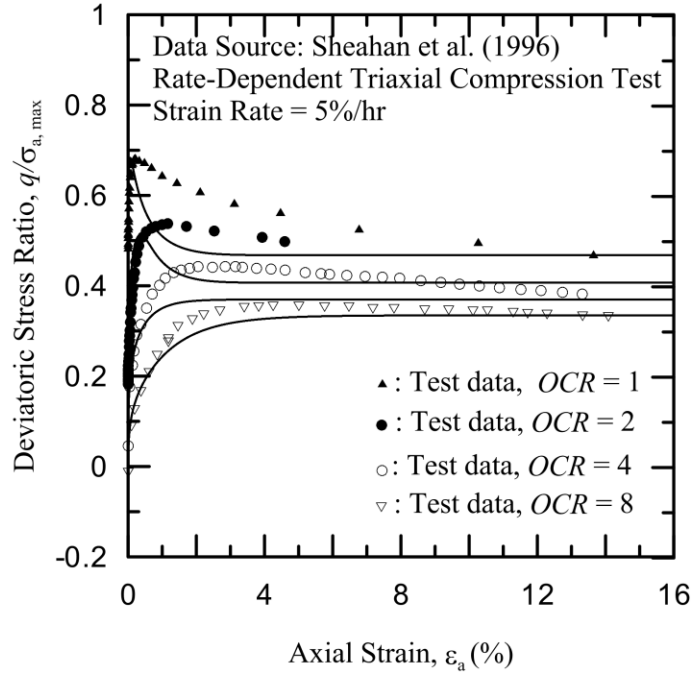
(b)

Figure 6. Rate-independent, isotropically consolidated triaxial compression test results for London clay: (a) stress strain plot and (b) stress path plot (test data from Gasparre 2005)

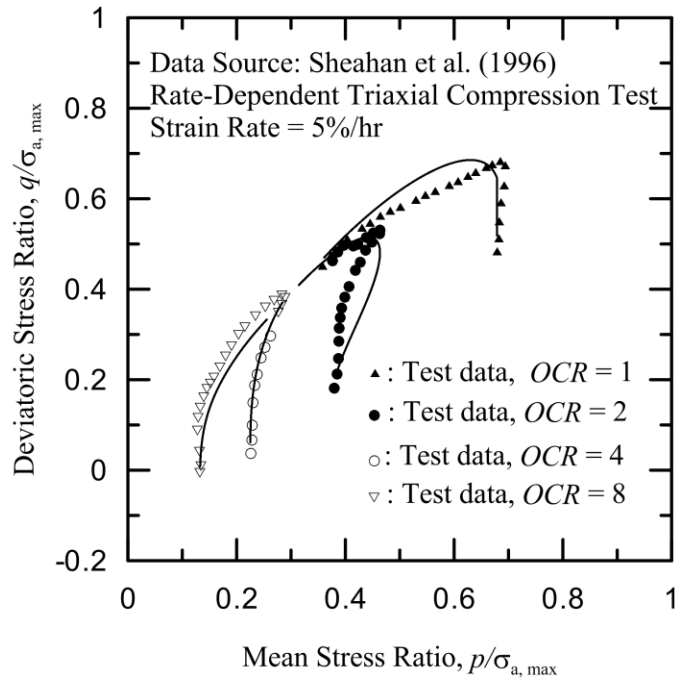
### ***Undrained Rate-Dependent Behavior***

Figure 7 shows the comparison between simulation and experimental results of rate-dependent,  $K_0$ -consolidated triaxial compression tests on BBC with an applied strain rate of 5%/hr. The stresses are normalized with respect to the maximum axial stress  $\sigma'_{a,max}$ . The stress-strain (Figure 7(a)) and stress path plots (Figure 7(b)) demonstrate the ability of the constitutive model to capture the mechanical response of clays under strain rate-dependent loading. The model captures the peak undrained strength  $s_{u,peak}$  as a function of strain rate reasonably well for the range of  $OCR$  considered in the study. The post-peak shear strength is, however, under predicted. The stress paths are also captured with reasonable accuracy. Similar comparisons for BBC for other strain-rate values are given in Martindale (2011).

Figure 8 shows the deviatoric stress versus axial strain plots of rate-dependent, isotropically consolidated triaxial tests performed on LC samples with  $OCR = 1$  and 5 at different strain rates. The simulated plots are in reasonable agreement with the experimental plots. Similar comparisons for KC were also done the details of which are given in Martindale (2011). Figure 9 shows the plots of the predicted  $s_{u,peak}$  values for BBC, LC and KC along with the corresponding experimental values as a function of strain rate. This plot shows that the developed constitutive model predicts the rate-dependent undrained shear strength of clay reasonably well.



(a)



(b).

Figure 7. Rate-dependent,  $K_0$  consolidated triaxial compression test results for Boston Blue clay (applied strain rate = 5%/hr): (a) stress strain plot and (b) stress path plot (test data from Sheahan et al. 1996)

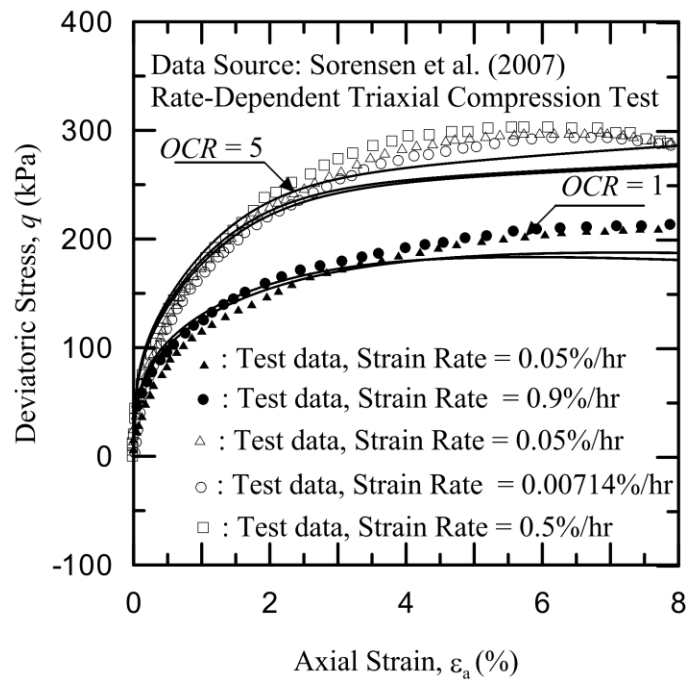
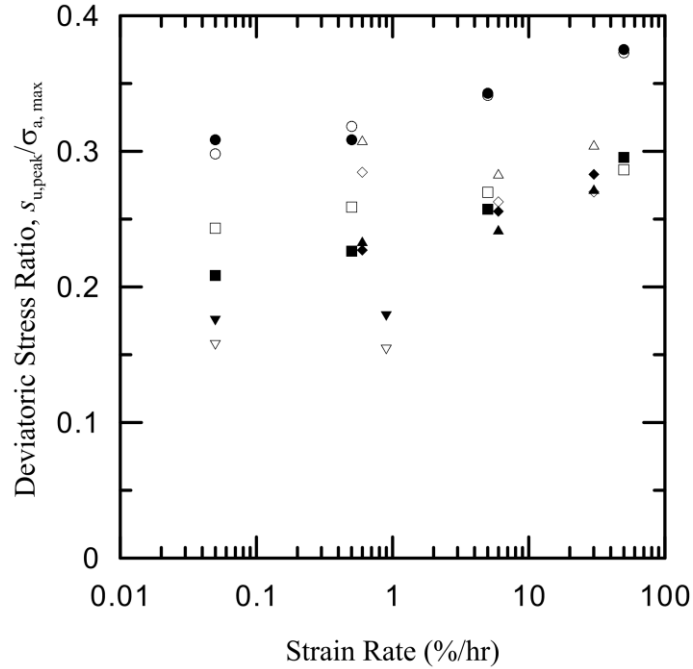


Figure 8. Stress strain plots for rate-dependent, isotropically consolidated triaxial compression tests performed on London clay (test data from Sorensen et al. 2007)



Boston Blue Clay

- Simulation,  $OCR = 1$
- Test data,  $OCR = 1$  (Sheahan et al. 1996)
- Simulation,  $OCR = 2$
- Test data,  $OCR = 2$  (Sheahan et al. 1996)

Kaolin Clay

- ◆ Simulation,  $OCR = 1$
- ◇ Test data,  $OCR = 1$  (Mukabi and Tatsuoka 1999)
- ▲ Simulation,  $OCR = 1.2$
- △ Test data,  $OCR = 1.2$  (Mukabi and Tatsuoka 1999)

London Clay

- ▼ Simulation,  $OCR = 1$
- ▽ Test data,  $OCR = 1$  (Sorensen et al. 2007)

Figure 9. Normalized  $s_{u,peak}$  as a function of strain rate: comparison of simulation and experimental results

***Parametric Sensitivity Study***

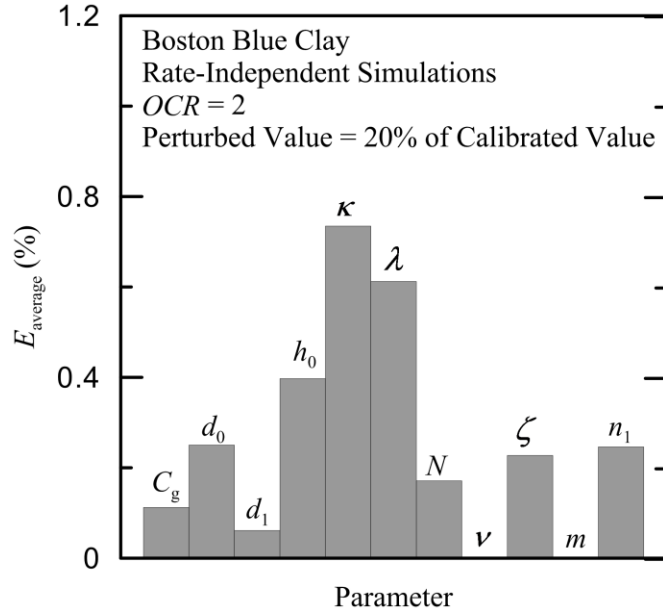
The sensitivity of each model parameter was checked for BBC, LC and KC. For the sensitivity study, the model parameters were perturbed by  $\pm 20\%$  of their calibrated values one at a time. An average error  $E_{average}$  was calculated for each parameter as

$$E_{\text{average}} (\%) = \left[ \frac{\sum_{i=1}^{\text{Total Number of Strain Values}} \left[ \frac{|q_{\text{base},i} - q_{\text{var},i}|}{q_{\text{base},i}} \times 100 \right]}{\text{Total Number of Error Calculations at Different Strain Values}} \right] \quad (28)$$

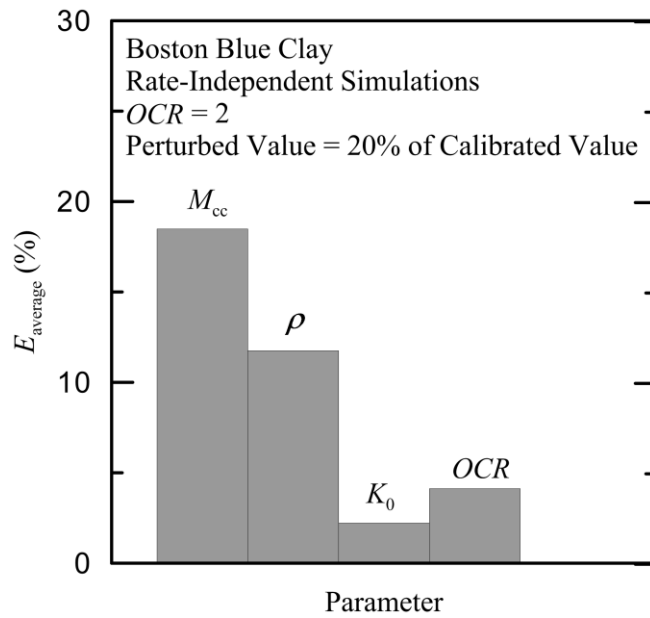
where  $q_{\text{base},i}$  is the value of deviatoric stress obtained from model simulation at  $i^{\text{th}}$  strain increment using the calibrated model parameters and  $q_{\text{var},i}$  is the corresponding value of deviatoric stress obtained from model simulation when a parameter is perturbed. The error  $E = |q_{\text{base},i} - q_{\text{var},i}|/q_{\text{base},i}$  is calculated at different strain values and then the total accumulated error for all the strain values is divided by the number of calculations to obtain  $E_{\text{average}}$ .  $E_{\text{average}}$  calculated for all the parameters of BBC for rate-independent,  $K_0$  consolidated triaxial test simulations are shown in Table 4 for different values of  $OCR$ . The values corresponding to  $OCR = 2$  and +20% perturbation are shown in Figure 10. It is evident that  $M_{\text{cc}}$ ,  $\rho$ ,  $OCR$  and  $K_0$  are the most sensitive parameters. For normally consolidated clays,  $\lambda$  and  $\kappa$  are relatively more sensitive than the remaining parameters while, for overconsolidated clays, the dilatancy parameters  $d_0$  and  $d_1$  are relatively more sensitive. Similar trends were observed for LC and KC as well (Martindale 2011).

Table 4. Average Parameter Sensitivity Error for Boston Blue Clay for Rate-Independent Loading

Average Parameter Sensitivity Error $E_{\text{average}}$ (%)								
Parameter	+20% Variation				-20% Variation			
	$OCR = 1$	$OCR = 2$	$OCR = 4$	$OCR = 8$	$OCR = 1$	$OCR = 2$	$OCR = 4$	$OCR = 8$
$C_g$	0.15	0.11	0.50	0.82	0.19	0.14	0.60	0.96
$d_0$	0.83	0.25	0.51	2.64	1.33	0.39	0.75	3.39
$d_1$	0	0.06	0.39	4.27	0	0.06	0.35	34.55
$M_{cc}$	17.89	18.54	19.46	22.64	18.68	19.01	19.87	22.67
$h_0$	0.39	0.39	0.48	0.27	0.55	0.56	0.73	0.39
$\kappa$	2.94	0.73	1.58	4.21	3.01	0.77	1.82	5.30
$\lambda$	2.09	0.61	0.58	1.09	3.26	0.93	0.85	1.73
N	0.11	0.17	0.53	1.38	0.12	0.16	0.54	1.36
$\rho$	11.22	11.802	11.75	12.38	17.03	18.08	18.18	20.89
$\nu$	0	0	0	0	0	0	0	0
$\zeta$	0.39	0.22	1.25	2.26	0.56	0.25	1.69	3.76
$K_0$	9.14	2.27	2.62	3.72	10.14	2.52	2.70	3.26
$OCR$	4.33	4.18	5.77	11.89	-	5.29	6.44	12.51
$m$	0.01	0	0	0	0	0	0	0
$n_1$	0.40	0.24	0.08	0.11	0.48	0.28	0.09	0.12



(a)



(b)

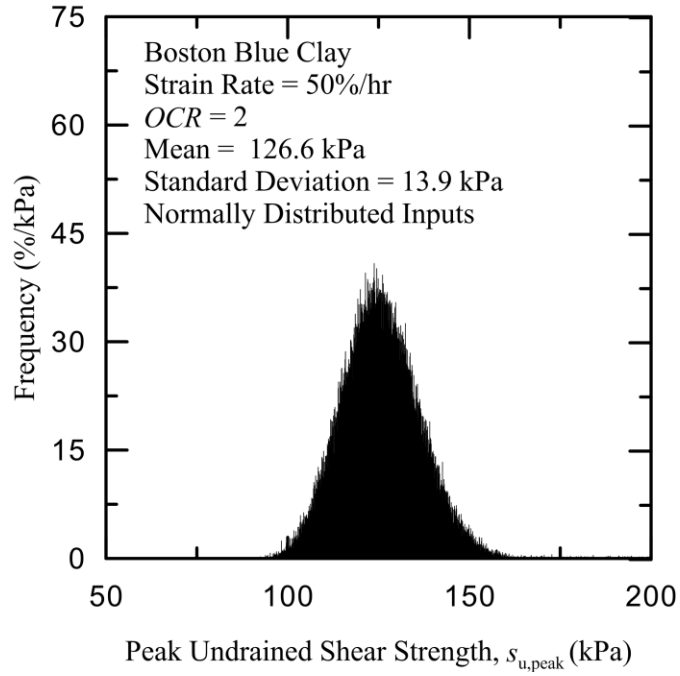
Figure 10. Average normalized cumulative error  $E_{\text{average}}$  for +20% variation of model parameters of Boston Blue Clay for rate-independent,  $K_0$  consolidated triaxial simulations at  $OCR = 2$ : (a) parameters with low sensitivity and (b) parameters with high sensitivity



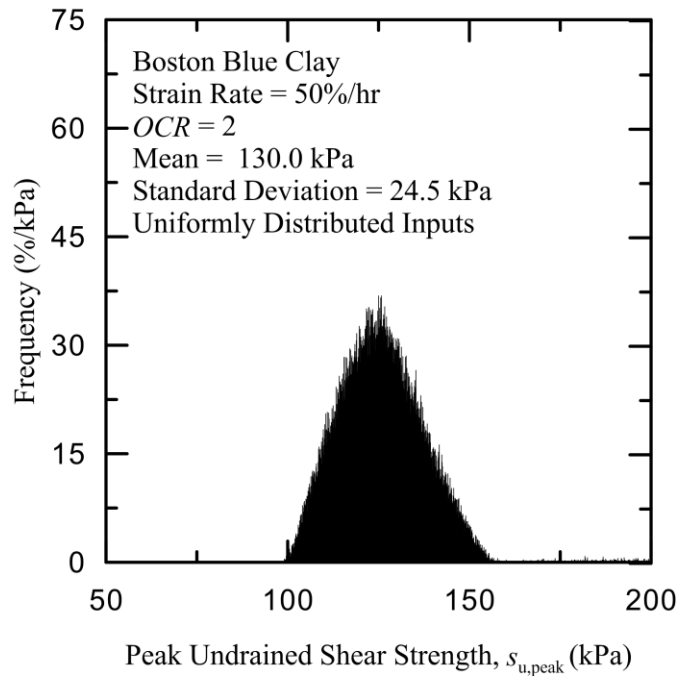
### ***Uncertainties in Model Parameters***

The uncertainty associated with the estimation of the model parameters is investigated probabilistically by considering the model parameters as random variables and performing Monte Carlo (M-C) simulations of the mechanical response of BBC. The study was done assuming that the random variables (model parameters) follow normal and uniform probability distributions. The calibrated deterministic values were assumed to be the means  $\mu$  of the random parameters. The standard deviations  $\sigma$  were calculated with the assumption that the  $\pm 20\%$  scatter about the mean (deterministic) values correspond to  $\pm 3\sigma$ . Thus, the coefficient of variation COV ( $= \sigma/\mu$ ) for all the parameters is 0.067. The same mean and standard deviation values were used for normal and uniform distributions in the M-C simulations.

Representative histograms of  $s_{u,peak}$  of BBC considering normal and uniform probability distribution functions are shown in Figure 11. These results were obtained for triaxial simulations at 50%/hr strain rate on  $K_0$  consolidated specimens with  $OCR = 2$ . The nature of the distributions of  $s_{u,peak}$  is approximately the same for both the normal and uniform probability distributions of the input parameters. The difference in the mean values of  $s_{u,peak}$  obtained for normally and uniformly distributed input parameters is only 0.21%. A similar trend was observed for the undrained shear strength  $s_{u,CS}$  at the critical state (Martindale 2011).



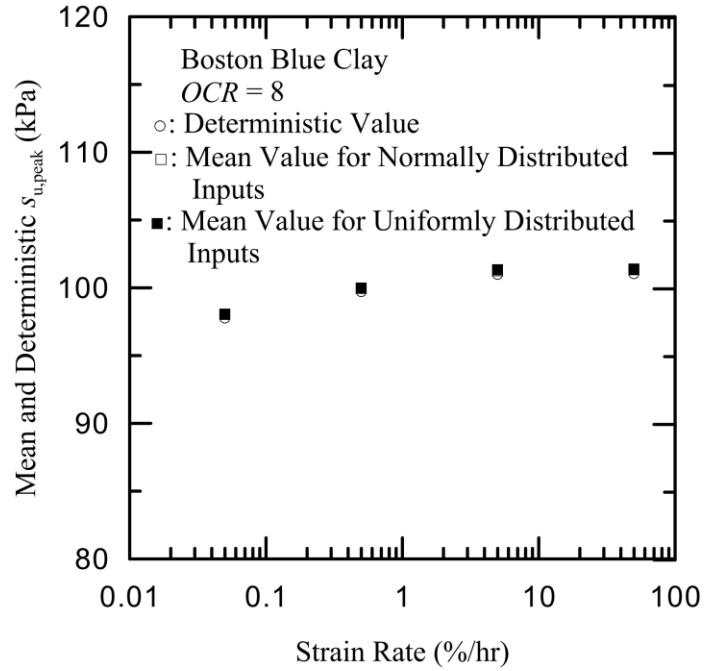
(a)



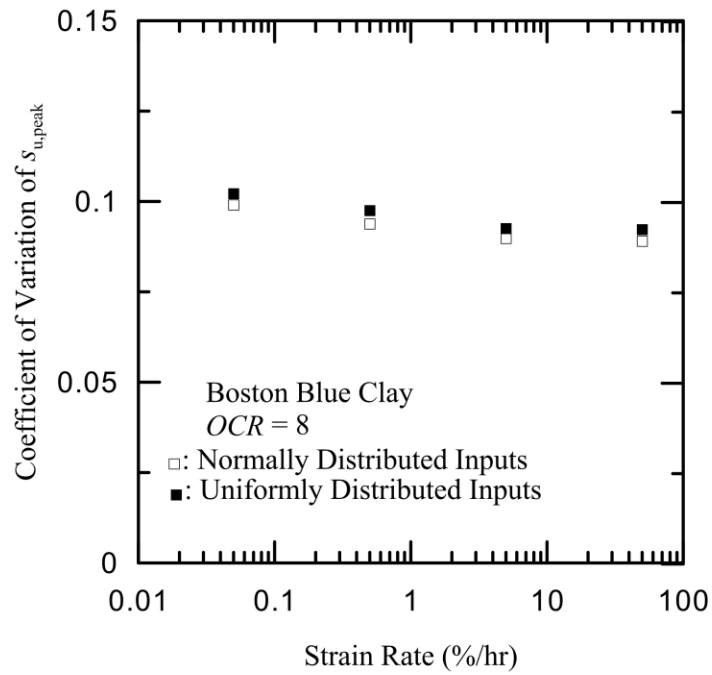
(b)

Figure 11. Histogram of  $s_{u,peak}$  obtained using (a) normal and (b) uniform probability distribution functions for the model parameters

Figure 12 shows the mean and COV of  $s_{u,peak}$  of  $K_0$  consolidated BBC at  $OCR = 8$  as a function of strain rate. The  $s_{u,peak}$  values are obtained deterministically and probabilistically using normally and uniformly distributed inputs. The mean values for all the three cases match very well. The mean (or deterministic) undrained shear strength increases while the COV decreases with increase in the applied strain rate. Figure 12(a) shows that the deterministic and mean values are the same for practical purposes. Figure 12(b) indicates that, in most likelihood, the magnitude of error in the estimation of the undrained shear strength due to erroneous model parameter estimations will not be significant.



(a)



(b)

Figure 12. Variation of (a) mean and deterministic  $s_{u,peak}$  and (b) COV of  $s_{u,peak}$  with applied strain rate for  $OCR = 8$

## CONCLUSIONS

The report presents a rate-dependent plastic constitutive model for clays developed using the concepts of critical state soil mechanics and bounding surface plasticity. The model consists of conical yield, dilatancy and critical state surfaces with a flat cap on the critical state surface. The model is capable of simulating clay behavior for both isotropic and anisotropic initial stress state and for loading paths that are more general than triaxial compression/extension. The proposed model has 1 rate dependent parameter and 14 rate independent parameters. The parameters were determined for BBC, LC and KC following a hierarchical manner. The model considers *OCR* dependent model calibration process for the strain-rate dependent parameter.

The proposed constitutive model captures adequately the rate-independent and rate-dependent response of clay behavior under isotropic and  $K_0$ -consolidated triaxial compression conditions. The model retains the rate-independent formulation in conjunction with the two-surface plasticity model and simulates the rate-dependent clay response without expensive numerical algorithm.

The sensitivity of each model parameter is checked by perturbing the calibrated values by  $\pm 20\%$  one at a time. The parameters  $M_{cc}$ ,  $\rho$ , *OCR* and  $K_0$  are the most sensitive. For normally consolidated clays,  $\lambda$  and  $\kappa$  are relatively more sensitive than the remaining parameters while, for overconsolidated clays, the dilatancy parameters  $d_0$  and  $d_1$  are relatively more sensitive.

The uncertainties associated with the estimation of the model parameters was investigated probabilistically by considering the model parameters as random variables following normal and uniform probability distributions. Monte Carlo (M-C) simulations

were performed and the statistics of the undrained shear strength of BBC was investigated. The same values of mean and standard deviation were used for normal and uniform distributions in the M-C simulations. The  $s_{u,peak}$  values, obtained deterministically and probabilistically using normally and uniformly distributed inputs, matched very well. The coefficients of variation of  $s_{u,peak}$  were found to be not more than 12% which indicate that the magnitude of error in the estimation of the undrained shear strength due to erroneous model parameter estimations will not be significant.

## REFERENCES

- Adachi, T. and Oka, F. (1982). "Constitutive equations for normally consolidated clay based on elasto-viscoplasticity." *Soils and Foundations*, 22(4), 57-70.
- Been, K. and Jefferies, M. G. (1985). "A State Parameter for Sands." *Géotechnique*, 35(2), 99-112.
- Chakraborty, T. (2009). "Development of a clay constitutive model and its application to pile boundary value problems." *Ph.D. Thesis*, Purdue University, West Lafayette, Indiana, USA.
- Dafalias, Y. F. (1982). "Bounding surface elastoplasticity-viscoplasticity for particulate cohesive media." *International Union of Theoretical and Applied Mechanics Conference on Deformation and Failure of Granular Materials* (P. A. Vermeer and H. J. Luger, eds.), 97-107.
- Dafalias, Y. F., Papadimitriou, A. G. and Li, X. S. (2004). "Sand plasticity model accounting for inherent fabric anisotropy." *Journal of Engineering Mechanics, ASCE*, 130(11), 1319-1333.

- Díaz-Rodríguez, J. A., Martínez-Vasquez, J. J. and Santamarina, J. C. (2009). “Strain-rate effects in Mexico city soil.” *Journal of Geotechnical and Geoenvironmental Engineering, ASCE*, 135(2), 300-305.
- Gasparre, A. (2005). “Advanced laboratory characterization of London clay.” *Ph.D. Thesis*, Imperial College London.
- Gasparre, A., Nishimura, S., Minh, N. A., Coop, M. R. and Jardine, R. J. (2007a). “The stiffness of natural London clay.” *Géotechnique*, 57(1), 33-7.
- Gasparre, A., Nishimura, S., Coop, M. R., and Jardine, R. J. (2007b). “The influence of structure on the behaviour of London clay.” *Géotechnique*, 57(1), 19-31.
- Hájek, V., Mašín, D., and Boháč, J. (2009). “Capability of constitutive models to simulate soils with different OCR using a single set of parameters.” *Computers and Geotechnics*, 36, 655-664.
- Hardin, B. O. (1978). “The nature of stress-strain behavior of soils.” State-of –the-Art Report, *Proceedings of the ASCE Specialty Conference on Earthquake Engineering and Soil Dynamics*, Pasadena, 1978, 3-90.
- Hight, D.W., McMillan, F., Powell, J. J. M., Jardine, R.J., and Allenou, C.P. (2003). “Some characteristics of London clay.” *Characterization of Engineering Properties of Natural Soils*, Balkema, 851-908.
- Hinchberger S. D. and Rowe, K. R. (1998). “Evaluation of the predictive ability of two elasticviscoplastic constitutive models.” *Canada Geotechnical Journal*, 35, 769–789.
- Jung, B. C. and Biscontin, G. (2006). “Modeling of strain rate effects on clay in simple shear.” *Proceedings of GeoCongress 2006*, 1-6.

- Kaliakin, V. N. and Dafalias, Y. F. (1990a). "Theoretical aspects of the elastoplastic-viscoplastic bounding surface model for cohesive soils." *Soils and Foundations*, 30(3), 11-24.
- Kaliakin, V. N. and Dafalias, Y. F. (1990b). "Verification of the elastoplastic-viscoplastic bounding surface model for cohesive soils." *Soils and Foundations*, 30(3), 25-36.
- Kavazanjian, E., and Mitchell, J. K. (1980). "Time-dependent deformation behavior of clays." *Journal of Geotechnical and Geoenvironmental Engineering*, ASCE, 106(6), 611-630.
- Ladd, C. C. and Edgers, L. (1972). "Consolidated-Undrained Direct Simple Shear Tests on Boston Blue Clay." *Research Report R72-82*, Department of Civil Engineering, MIT, Cambridge, MA.
- Ladd, C.C. and Varallyay, J. (1965). "The influence of the stress system on the behavior of saturated clays during undrained shear." *Research Report No R65-11*, Department of Civil Engineering, MIT, Cambridge, MA.
- Leroueil, S., Tavenas, F., Samson, L. and Morin, P. (1983). "Preconsolidation Pressure of Champlain Clays – Part II: Laboratory Determination." *Canadian Geotechnical Journal*, 20(4), 803-816.
- Leroueil, S., Kabbaj, M., Tavenas, F. and Bouchard, R. (1985). "Stress-strain rate relation for the compressibility of sensitive natural clays." *Géotechnique*, 35(2), 159-180.
- Li, X. S. and Dafalias, Y. F. (2000). "Dilatancy of cohesionless soils." *Géotechnique*, 50(4), 449-460.



- Ling, H. I., Yue, D., Kaliakin, V. and Themelis, N.J. (2002). “An anisotropic elastoplastic bounding surface model for cohesive soils.” *Journal of Engineering Mechanics, ASCE*, 128(7), 748-758.
- Loukidis, D. and Salgado, R. (2009). “Modeling sand response using two-surface plasticity.” *Computers and Geotechnics*, 36, 166–186.
- Manzari, M. T. and Dafalias, Y. F. (1997). “A critical state two-surface plasticity model for sands.” *Géotechnique*, 47(2), 255-272.
- Martindale, H. (2011). “Rate-Dependent Behavior of Clay.” *M.S. Thesis*, University of Connecticut, Storrs, Connecticut, USA.
- Matešić, L. and Vucetic, M. (2003). “Strain-Rate Effect on Soil Secant Modulus at Small Cyclic Strains.” *Journal of Geotechnical and Geoenvironmental Engineering, ASCE*, 129(6), 536–549.
- Mukabi, J.N. and Tatsuoka, F. (1999) “Influence of reconsolidation stress history and strain rate on the behaviour of kaolin over a wide range of strain.” 12th ARC: Geotechnics for Developing Africa, Durban, South Africa., 365-377.
- Nishimura, S. (2005). “Laboratory study on anisotropy of natural London Clay.” *PhD Thesis*, Imperial College London.
- Ortiz, M. and Simo, J. C. (1986). “An Analysis of a New Class of Integration Algorithms for Elastoplastic Constitutive Relations.” 23, 353-366.
- Papadimitriou, A. G. and Bouckovalas, G. D. (2002). “Plasticity Model for Sand Under Small and Large Cyclic Strains: a Multiaxial Formulation.” *Soil Dynamics and Earthquake Engineering*, 22 (3), 191-204.

- Papadimitriou AG, Manzari MT and Dafalias YF. (2005) “Calibration of A Simple Anisotropic Plasticity Model for Soft Clays.” *Proceedings, GeoFrontiers Conference of ASCE, January 24–26, Austin, TX, Geotechnical Special Publication No. 128, 415–424.*
- Paquin, G. (1983). “Contribution à l’étude de la Déstructuration et Restructuration des Argiles Sensible.” *M.S. Thesis, Université Laval, Quebec, P.Q.*
- Perzyna, P. (1963). “The Constitutive Equations for Rate Sensitive Plastic Materials.” *Quarterly of Applied Mathematics, 20, 321-332.*
- Perzyna, P. (1966). “Fundamental Problems in Viscoplasticity.” *Advances in Applied Mechanics, 9, 244–377.*
- Pestana, J. M., Whittle, A. J. and Gens, A. (2002). “Evaluation of a Constitutive Model for Clays and Sands: Part II – Clay Behavior.”, *International Journal for Numerical and Analytical Methods in Geomechanics, 26, 1123-1146.*
- Prashant, A. (2004). “Three-Dimensional Mechanical Behavior of Kaolin Clay with Controlled Microfabric Using True Triaxial Testing.” *PhD. Dissertation, University of Tennessee, Knoxville, USA.*
- Sheahan, T.C. (1991). “An Experimental Study of the Time-Dependent Undrained Shear Behavior of Resedimented Clay Using Automated Stress Path Equipment.” *Doctoral Dissertation, MIT, Cambridge, MA.*
- Sheahan, T.C., Ladd, C.C. and Germaine, J.T. (1996). “Rate Dependent Undrained Shear Behaviour of Saturated Clay.” *Journal of Geotechnical and Geoenvironmental Engineering, ASCE, 122(2), 99–108.*

- Sheahan, T.C. (2005). "A Soil Structure Index to Predict Rate Dependence of Stress-Strain Behavior." *Testing, Modeling and Simulation in Geomechanics*, ASCE, Geotechnical Special Publication, no. 143, 81-97.
- Sorensen, K.K., Baudet, B. A. and Simpson, B. (2007). "Influence of Structure on the Time-Dependent Behaviour of a Stiff Sedimentary Clay." *Géotechnique*, 57(1), 113–124.
- Terzaghi, K., Peck, R. B. and Mesri, G. (1996). *Soil Mechanics in Engineering Practice*. 3rd Ed., Wiley, New York.
- Zhou, H. and Randolph, M.F. (2007). "Computational Techniques and Shear Band Development for Cylindrical and Spherical Penetrometers in Strain-Softening Clay." *International Journal of Geomechanics*, 7(4), 287–295.
- Zienkiewicz, O. C. and Corneau, I. C. (1974). "Viscoplasticity, Plasticity and Creep in Elastic Solids: A Unified Numerical Solution Approach." *International Journal of Numerical Methods in Engineering*, 8, 821–828.